Astron. Astrophys. 331, 651–660 (1998)

ASTRONOMY AND ASTROPHYSICS

Molecular gas phase counterparts to solid state grain mantles features: implication for gas/grain chemistry

E. Dartois[1], L. d'Hendecourt[1], F. Boulanger[1], M. Jourdain de Muizon[2,3], M. Breitfellner[4], J.-L. Puget[1], and H. J. Habing[5].

[1] IAS-CNRS, Université Paris XI, Batiment 121, F-91405 Orsay Cedex, France
[2] DESPA, Observatoire de Paris, F-92190 Meudon, France
[3] LAEFF-INTA, ESA Satellite tracking Station, P.O. Box 50727, E-28080 Madrid, Spain
[4] ISO Science Operations, ESA/VILSPA Satellite Tracking Station, P.O. Box 50727, E-28080 Madrid, Spain
[5] Leiden Observatory, P.O. Box 9513, 2300 RA Leiden, The Netherlands

Received 24 April 1997 / Accepted 20 August 1997

Abstract. We present ISO SWS (AOT6) observations of the protostellar object RAFGL 7009S. This source is particularly interesting for the characterisation of chemistry arising from grain surfaces and mantles, since the solid state features of many simple molecules such as $H_2O, CO, CO_2, {}^{13}CO_2$ and CH_4 are detected, together with weaker features not yet unambiguously identified.

Gas phase H_2O, CO_2, CH_4 and CO can also be seen superimposed on the much broader solid state features. We derive an estimate for the gas phase temperature around 50K. The gas to solid ratios of these simple molecules is found to be $\geq$0.2 for H_2O, $\sim$0.2 for CH_4, and an order of magnitude lower for CO_2. We discuss the possible implications for interstellar chemistry in such objects.

Key words: ISM: RAFGL 7009S – ISM: molecules – dust, extinction – molecular processes – ISM: infrared: lines and bands

1. Introduction

The observation of a young star deeply embedded in a dense condensation is a powerful means of studying gas and grain chemistry. The new star provides a background source which allows us to probe cold matter in absorption in both the gas and on grains. Surface reactions and UV photoprocessing of icy mantles adsorbed on the grains are important processes for interstellar chemistry (d'Hendecourt et al. 1986). Such processes can be analysed and understood by comparing the observations to laboratory simulations which allow the precise reproduction of interstellar spectra. Simple interstellar gas phase molecules such as H_2O and CO_2 have not been extensively observed in the infrared with ground based telescopes because their rovibrational transitions are hidden by strong telluric absorption. Furthermore, linear and symmetric molecules present weak radio transitions and their abundances can therefore only be inferred from chemical models, or through the products of their reactions detectable at radio wavelength. For example, prior to ISO observations, the CO_2 gas phase abundance was inferred from observations of related ions such as HCO_2^+ in SgrB2 (Minh et al. 1988).

In this article we present ISO observations of the pre-main sequence star RAFGL 7009S. This source was initially chosen because its IRAS-LRS spectrum shows a strong feature around 15 μm attributed to the CO_2 bending mode in ice. The observation of this bending mode was first reported by d'Hendecourt & Jourdain de Muizon (1989) in the IRAS-LRS spectra of three protostellar objects. The first results we obtained on RAFGL 7009S with ISO (d'Hendecourt et al.,1996) were the identification of solid state molecular features of various infrared active modes in $H_2O, CO, CO_2, {}^{13}CO_2, CH_4$, "$XCN$", as well as a deep and broad absorption feature at 6.8 μm whose origin at the present time is still controversial. The "silicate" bands at 9.7 (saturated) and 18 μm are also prominent in this object. We complement these first results with higher resolution observations showing the rovibrational lines of gas phase H_2O, CO, CO_2 and CH_4. Solid state column densities for the identified molecules were deduced and will be discussed hereafter together with the gas phase component.

We use the extensive HITRAN rovibrational lines database (Rothman et al, 1996) as well as our own laboratory spectra to help us to disentangle the gas phase lines from the solid state features. We then derive the abundances of these molecules in both the gas and solid phases and discuss possible implications for the chemistry in protostellar environments.

2. Observations

Our observations of RAFGL 7009S include a full spectrum covering the wavelength range from $2.5 < \lambda < 45$ μm with a spec-

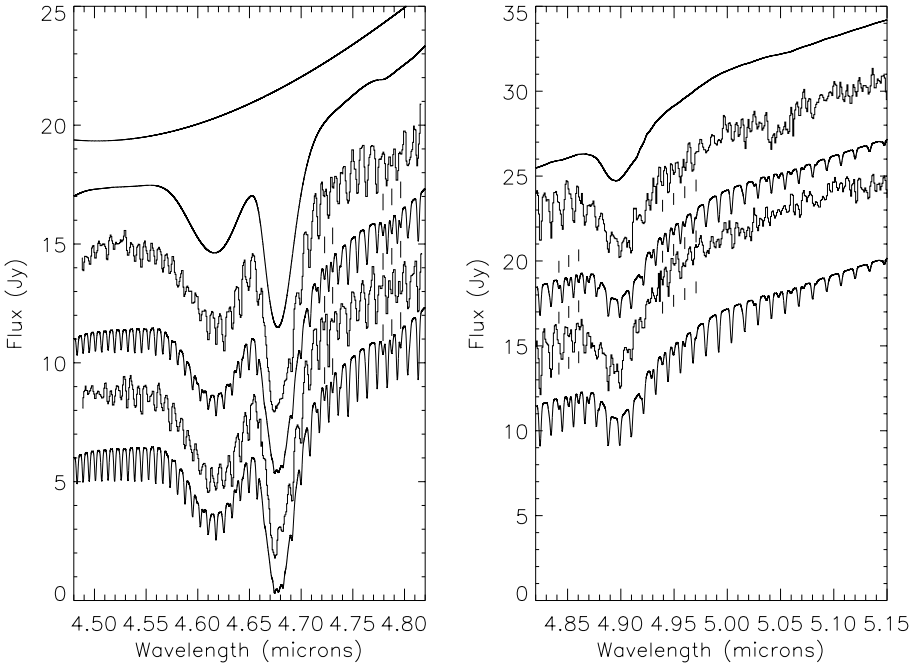

Fig. 1. Gas phase CO rovibrational transitions and ice features at 4.9 μm (tentatively attributed to "OCS", Geballe et al. 1985), 4.62 μm ("XCN") and solid CO at 4.67 μm. Left panel, from upper to lower curve: continuum adopted; solid state spectrum obtained in the laboratory from an irradiated ice at 13K containing CO and NH_3 multiplied by the adopted continuum; upward scans from ISO-SWS06 observation; composite spectrum built using the adopted continuum, gas phase model 1 described in Table 1 (including ^{12}CO and ^{13}CO components at T=40K and 740K (see rotational diagram) assuming a ^{13}CO/^{12}CO ratio of 60) and solid state spectrum from the laboratory; downward scans from ISO-SWS06 observation; composite spectrum built using the adopted continuum, gas phase model 2 described in table1 and solid state spectrum from the laboratory. Right panel, from upper to lower curve: adopted continuum (as the laboratory data do not fully reproduce this solid feature); upward scans from ISO-SWS06 observation; gas phase model 1 as presented above multiplied by the adopted continuum; downward scans from ISO-SWS06 observation; gas phase model 1 as presented above multiplied by the adopted continuum. Straight lines denote ^{13}CO transitions that are seen due to a good separation from ^{12}CO transitions. These models can be considered as the high column density cases.

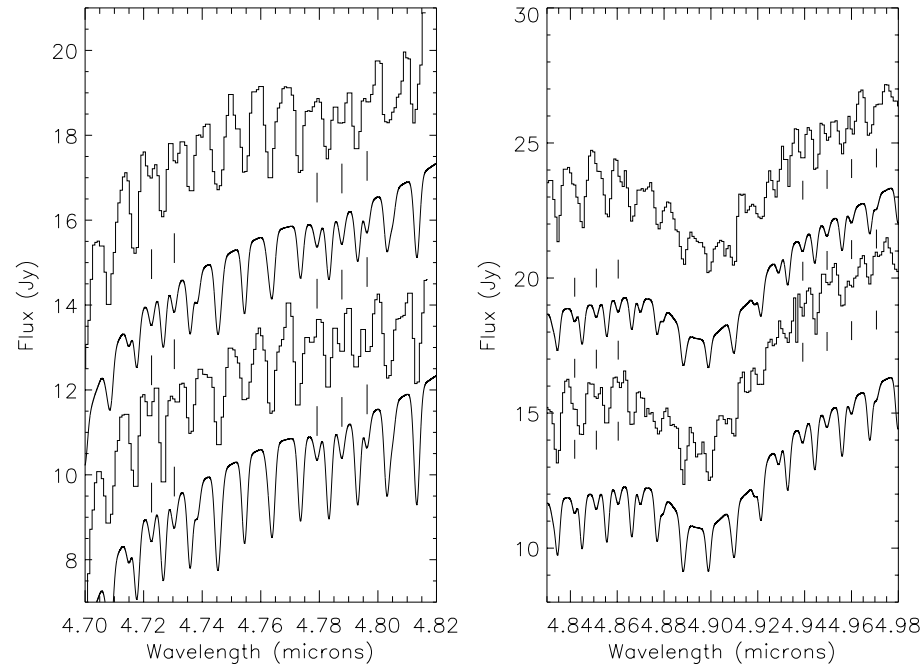

Fig. 2. A close-up of part of Fig. 4 showing the ^{13}CO sub-structures.

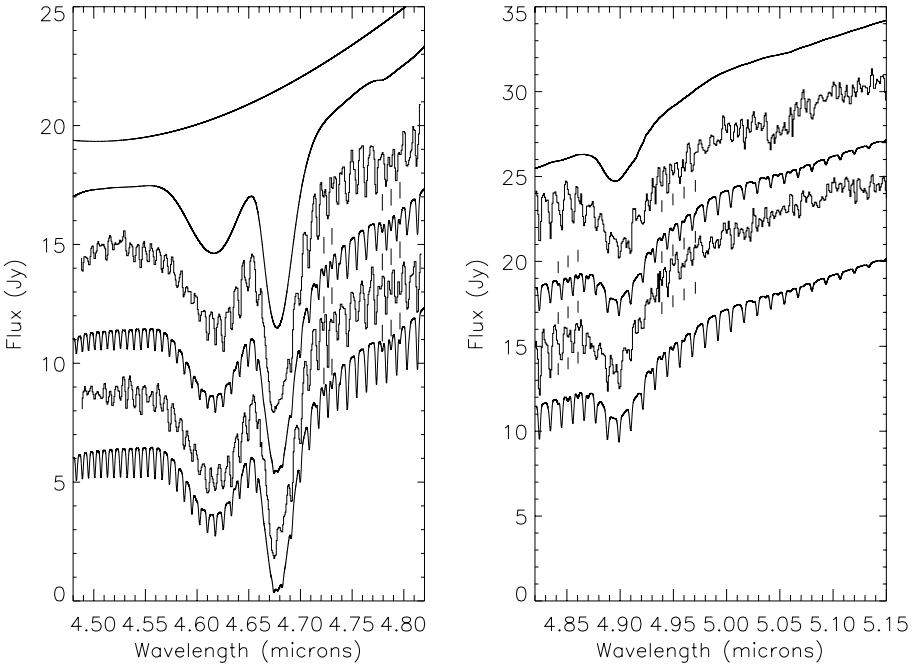

Fig. 3. Same figure as the Fig. 4 but using gas phase models 3 and 4 of Table 1. These models can be considered as the low column density cases.

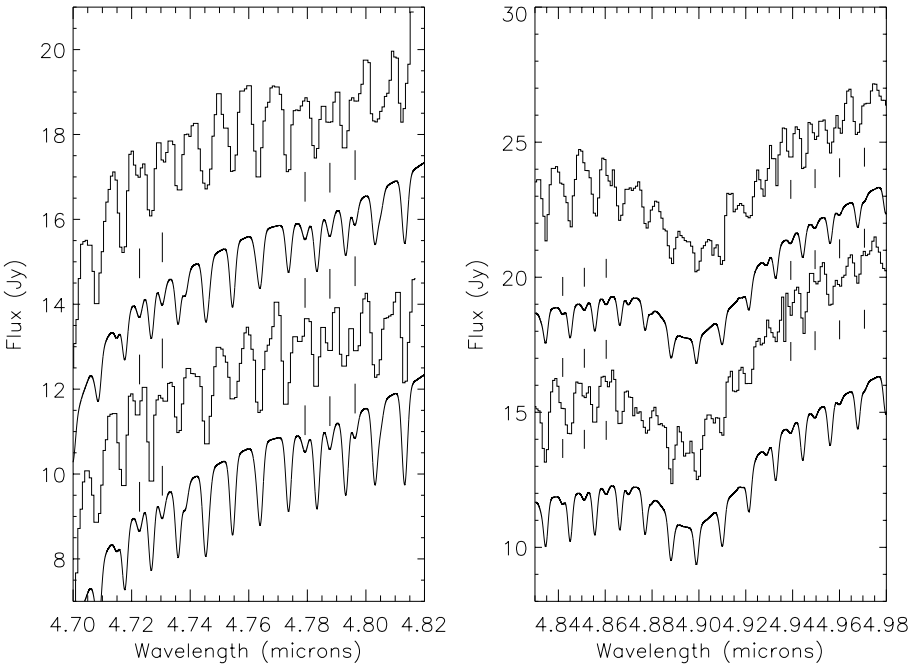

Fig. 4. A close-up of Fig. 6 showing the ^{13}CO sub-structures.

tral resolution of about 300 using the AOT(Astronomical Observation Template) SWS01 at speed 3, and higher resolution spectra over limited wavelength ranges (AOT SWS06). These spectra were obtained with the Short Wavelength Spectrometer (SWS, de Graauw et al. 1996) on board of ISO (Kessler et al. 1996). The data reduction procedures were performed with the Interactive Analysis (IA) software as installed at the ISO Science operation centre in VILSPA and IAS, and the final spectra were rebinned to a resolution of 1500 to 2000 for the AOT SWS06.

3. Results

3.1. Gas phase CO band

We observe the rovibrational transitions of CO in RAFGL 7009S between 4.5 and 5.15 μm as well as the solid state features falling in that range ("XCN" at 4.62 μm, solid CO at 4.67 μm, and a feature attributed to OCS at 4.9 μm (Geballe et al. 1985)). The spectra obtained with ISO are presented in Fig. 1-4, as well as the model and laboratory data used in their interpretation. In order to assess the nature of the features we have divided the ISO-SWS scans in two parts, upward

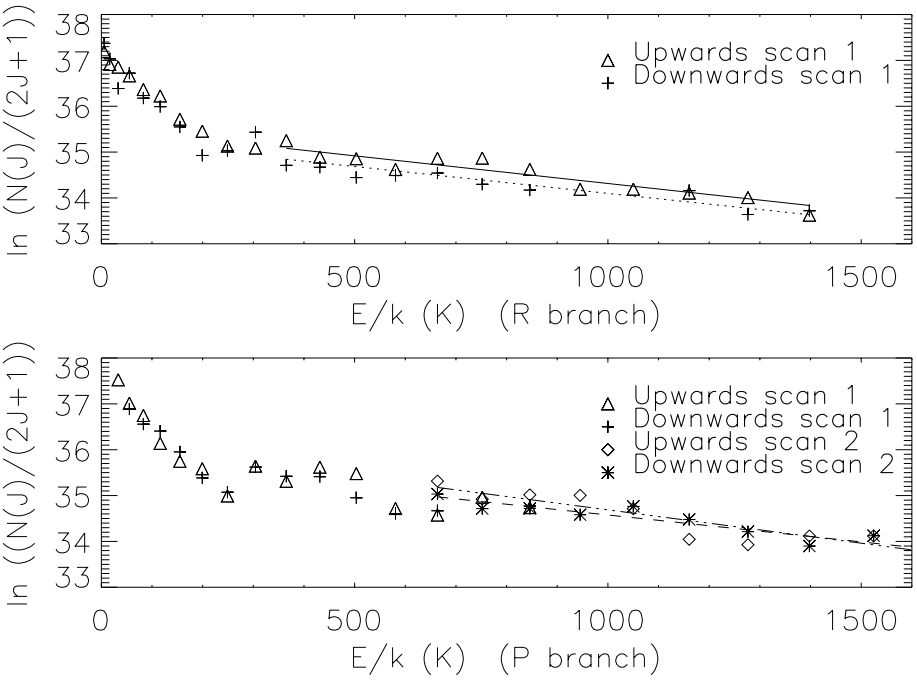

Fig. 5. ^{12}CO rotational diagrams (see text). The upper diagram is for the R branch on upward and downward scan directions. In this way, we take account of statistic effects for the separate scans without averaging. The same is done for the P branch but here data from two different observations are plotted (see left and right panel of Fig. 1.). Temperature derived is 740K $\pm$ 255K (3σ).

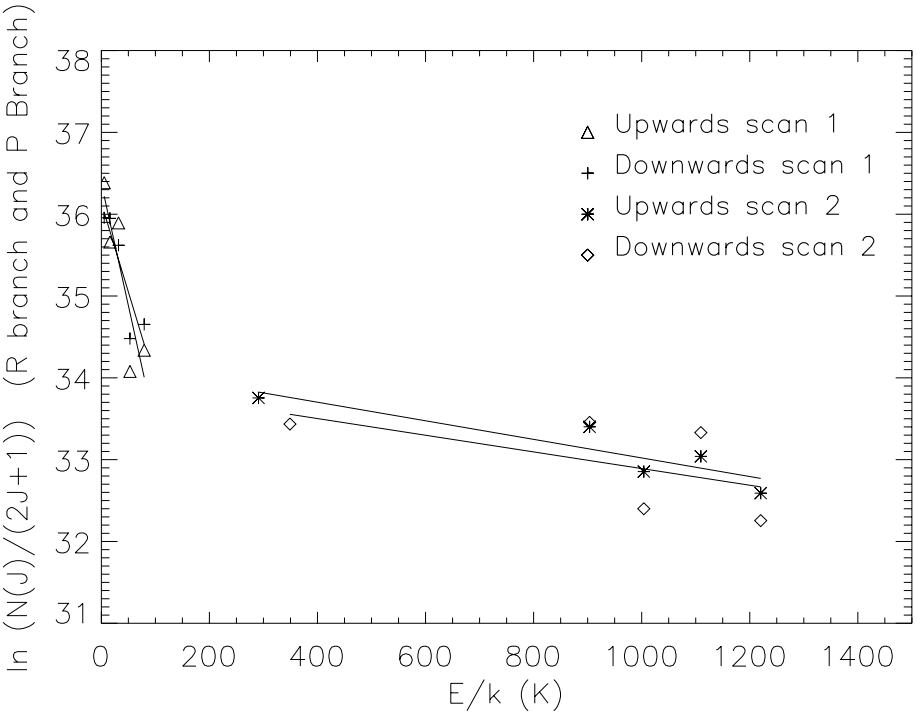

Fig. 6. ^{13}CO rotational diagrams. The diagram is for R branch and P branch upward and downward scan directions, on data from two different observations. The temperature derived is 40K $\pm$ 27K (3σ) for a cold component. For the hot component we find 900K $\pm$ 300K (3σ) with larger uncertainties due to the poorer statistics. However, the value for the hot component is compatible with the temperature inferred from the ^{12}CO data.

Table 1. Gas phase CO estimates and models used in Figs. 4-7).

$Molecule$	$^{12}COmolec.cm^{-2}$	$^{13}COmolec.cm^{-2}$	$^{12}COmolec.cm^{-2}$	$^{13}COmolec.cm^{-2}$
$Gas\ estimates$		$2.1 \times 10^{17} \pm 0.9(1\sigma)$		$9.7 \times 10^{16} \pm 2.4(1\sigma)$
$Temperature\ estimates$	$740K \pm 255K$			$40K \pm 27K$
$Temperature\ used$	$740K$	$740K$	$40K$	$40K$
$Model1$	$1.8 \times 10^{19}(3km.s^{-1})$	$3 \times 10^{17}(3km.s^{-1})$	$7.2 \times 10^{18}(3km.s^{-1})$	$1.2 \times 10^{17}(3km.s^{-1})$
$Model2$	$1.8 \times 10^{19}(5km.s^{-1})$	$3 \times 10^{17}(5km.s^{-1})$	$7.2 \times 10^{18}(3km.s^{-1})$	$1.2 \times 10^{17}(3km.s^{-1})$
$Model3$	$7.2 \times 10^{18}(3km.s^{-1})$	$1.2 \times 10^{17}(3km.s^{-1})$	$4.4 \times 10^{18}(3km.s^{-1})$	$7.3 \times 10^{16}(3km.s^{-1})$
$Model4$	$7.2 \times 10^{18}(5km.s^{-1})$	$1.2 \times 10^{17}(5km.s^{-1})$	$4.4 \times 10^{18}(3km.s^{-1})$	$7.3 \times 10^{16}(3km.s^{-1})$

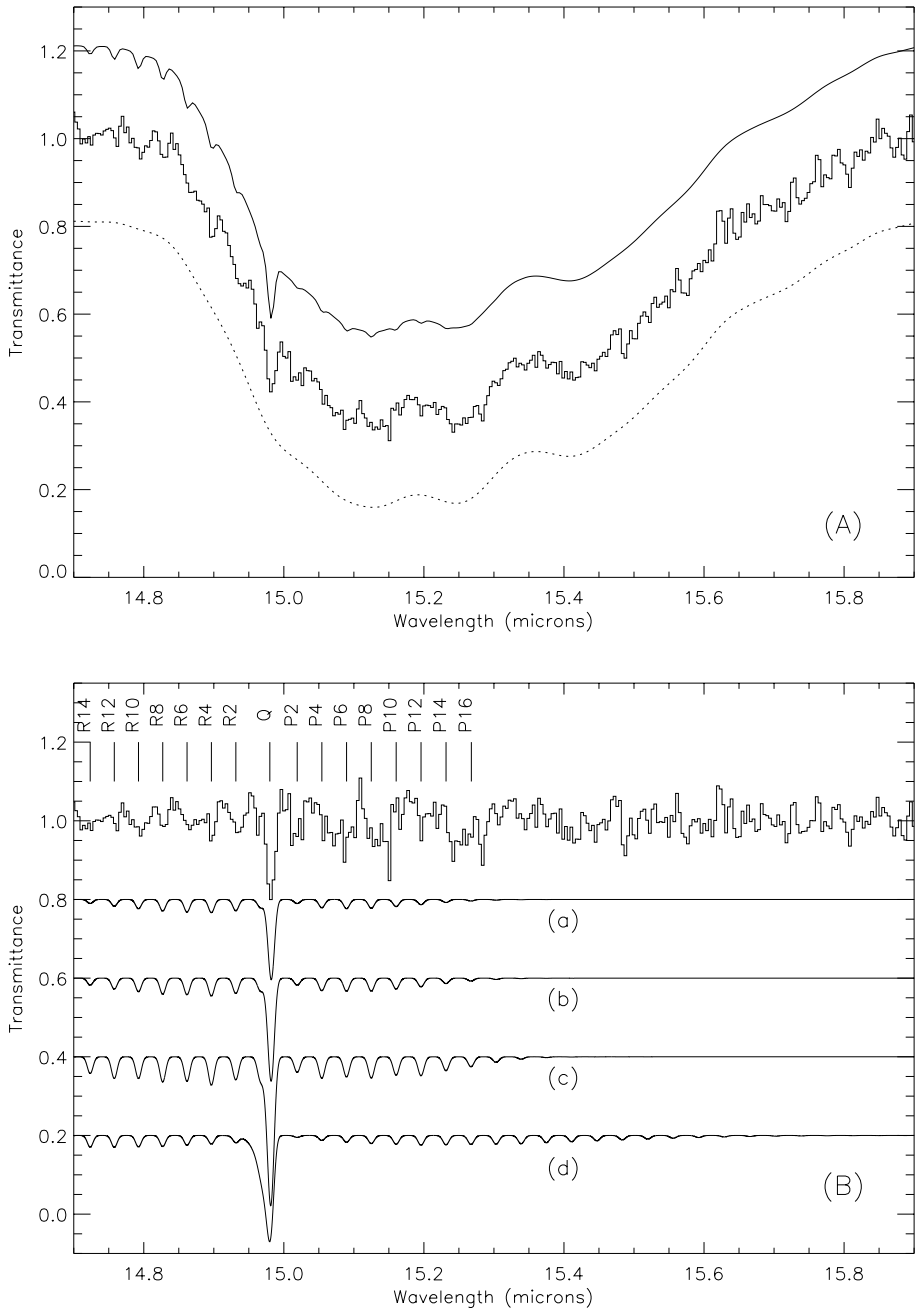

Fig. 7a and b. Gas phase CO_2 ν_2 band observed in RAFGL 7009S together with model spectra. **a** model spectra with gas (1×10^{17} molecule.cm^{-2}) and solid phase (upper curve), ISO SWS06 data (middle curve) and adopted solid phase transmittance (lower curve). **b** ISO transmittance spectrum after removal of the solid phase "baseline" and model spectra with v = 3 km.s^{-1}, T=40K and (a) 5×10^{16} molecule.cm^{-2}, (b) 1×10^{17} molecule.cm^{-2} , (c) 5×10^{17} molecule.cm^{-2}, (d) T=200K and 1×10^{17} molecule.cm^{-2}. The vertical lines indicate the various transitions involved.

and downward wavelength scanning, thus reducing by a small factor ($\sqrt{2}$) the signal-to-noise ratio and then having two spectra to confirm the features. This is particularly useful in the case of the ^{13}CO transitions as they are weak, but are clearly seen in the two scans and the models. Using rotational diagrams, depicted in Fig. 5 and 6, we estimate the excitation temperature of the gas. These diagrams use the fact that N$_J$, the number of molecules involved in a transition from the J level is proportional to $(2J + 1)\ e^{-E_J/kT}$. When ln(N$_J$/2J + 1) is plotted versus E_J/k, the slope of the fitted curve gives the excitation temperature of the gas (see for example Mitchell et al. 1990). For the high temperature, the high rotational levels of the ^{12}CO transition were used (see Fig. 5). These levels show a gas temperature of about 740 $\pm$ 255K (3σ). The low temperature component was determined using the ^{13}CO lines not blended with the main isotope. The scatter in values from the two different scans is quite large but gives a temperature of 40 $\pm$ 27K (3σ, see Fig. 6). Knowing these temperatures, we can then calculate the partition function $Q(T)$ for ^{13}CO (the high temperature for ^{13}CO is taken to be the same as that found for ^{12}CO) and make a diagram using N$_{total}$=N$_J$ $\times$ $Q(T)$ $\times$ $e^{E_J/kT}$/(2J + 1). Assuming that low J levels are dominated by the low temperature component and high levels by the high temperature component column densities are estimated. Total column densities in ^{13}CO arising from this study, as well as the different models gener-

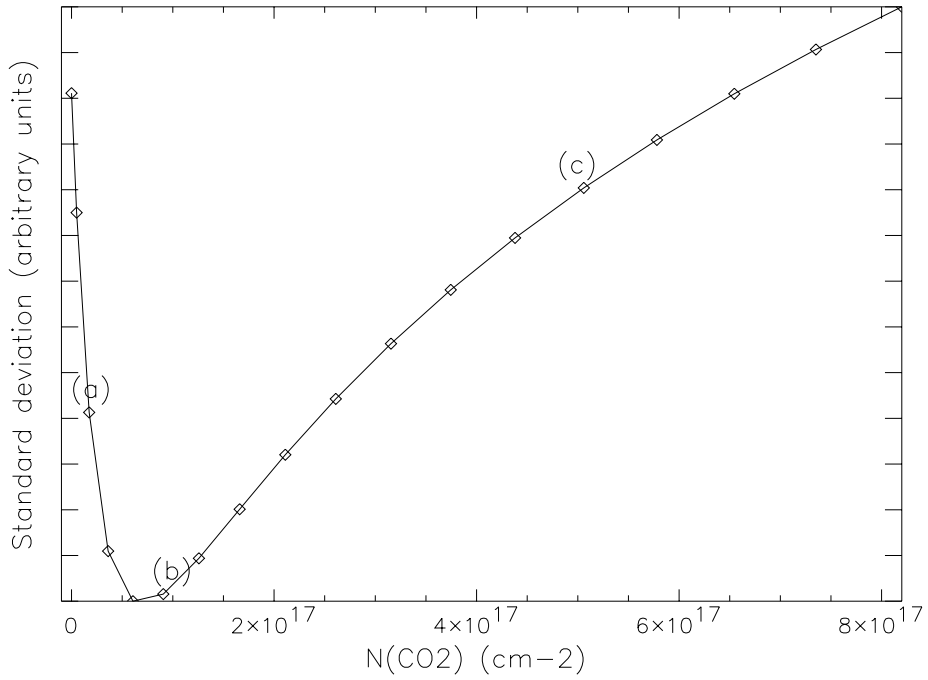

Fig. 8. Correlation diagram used to determine the CO_2 column density (see text). Letters (a),(b) and (c) correspond to the models presented in Fig. 7.

ated using a $^{12}CO/^{13}CO$ ratio of 60, and the error estimates are given in Table 1.

The high temperature is probably generated in a region close to the central object and may be related to an outflow or to interactions between the outflow and circumstellar matter (Shepherd and Churchwell 1996).

3.2. Gas phase CO_2 band

The ν_2 bending mode of CO_2 ($\Pi_u \leftarrow \Sigma_g^+$) is detected in the ISO spectrum of RAFGL 7009S and is slightly shifted compared to the CO_2 ice band, as previously published by van Dishoeck et al (1996). This result is shown in Fig. 7a, where the observations correspond to the middle trace. In addition to P and R branches, the CO_2 ν_2 mode presents a Q branch which shows transitions in the range 667.39 cm^{-1} to 672.18 cm^{-1} from J=2 up to J=68 and displays a single feature at the SWS resolution ($\sim$1500) which has a fairly strong integrated absorption coefficient.

Furthermore, due to the significant opacity present in the source, because of the high gas column density, P and R branches are also seen, although the P branch suffers from lower S/N in the region of the solid state absorption. A model was constructed using the HITRAN 96 database constants for the ν_2 bending mode line positions (Rothman et al 1996.) and Reichle and Young's integrated absorption coefficient (1972). We first use a Voigt profile for the lines with an adjustable Doppler FWHM given by the relation $\Delta\lambda = 2\sqrt{ln2}\lambda v/c$ where the turbulent velocity v is given in km s^{-1}, and the Lorentz profile given by the lifetime of the considered level, assuming an excitation temperature, T_{ex}, with LTE conditions in the gas. The extinction τ_λ is then obtained by summing the number of molecules involved in the transitions, multiplied by their integrated absorption coefficient distributed on the Voigt profile. Taking $e^{-\tau_\lambda}$ then produces the transmission spectrum. This yields the "infinite resolution" spectrum. We then convolve it with a gaussian having the ISO-SWS06 resolution to allow comparison with observations. The resultant spectrum is then compared to the observations after extraction of the continuum level and assuming a temperature (40K). We have few constraints on the exact temperature of the gas but we can exclude a 200 K excitation temperature from the asymmetry it would produce in the Q branch as shown in Fig. 2b. A turbulent velocity of v = 3 km.s^{-1} is taken, based on various CO isotope radio lines ($^{13}C^{16}O$, $^{12}C^{18}O$, Mc Cutcheon et al,1991) and is typical for such environments. In Fig. 7, the upper panel (a) presents three transmittance spectra which correspond respectively to the model (upper), the SWS06 spectrum (middle), and solid phase transmittance (lower), estimated from Fourier filtering of the original signal. The lower panel is the comparison of the gas transmittance spectrum with different column densities for CO_2 as well as a higher temperature. The determination of the gas column density is performed in the following manner: we compute gas transmittance spectra with increasing number of CO_2 molecules in the line of sight and divide the ISO reduced spectrum by the expected transmittance from the model. We then calculate the variance of the division. The variance diminishes until it reaches a minimum governed by the signal-to-noise, column density and model (see Fig. 8). The best fit is obtained with $N_{CO_2} \approx 1^{+1}_{-0.5}.10^{17}$ molecules.cm^{-2}. The final result is given in Fig. 7a (upper trace) made using the solid phase estimate and the gas phase model spectrum presented just above. To derive the CO_2 ice column density we use the band strength given by Gerakines et al. (1995) and derive 2.5×10^{18} cm^{-2} as already reported in d'Hendecourt et al. (1996). Thus, the derived CO_2 gas to solid ratio is about 5×10^{-2}. This is similar to the value given by van Dishoeck et al (1996) for other

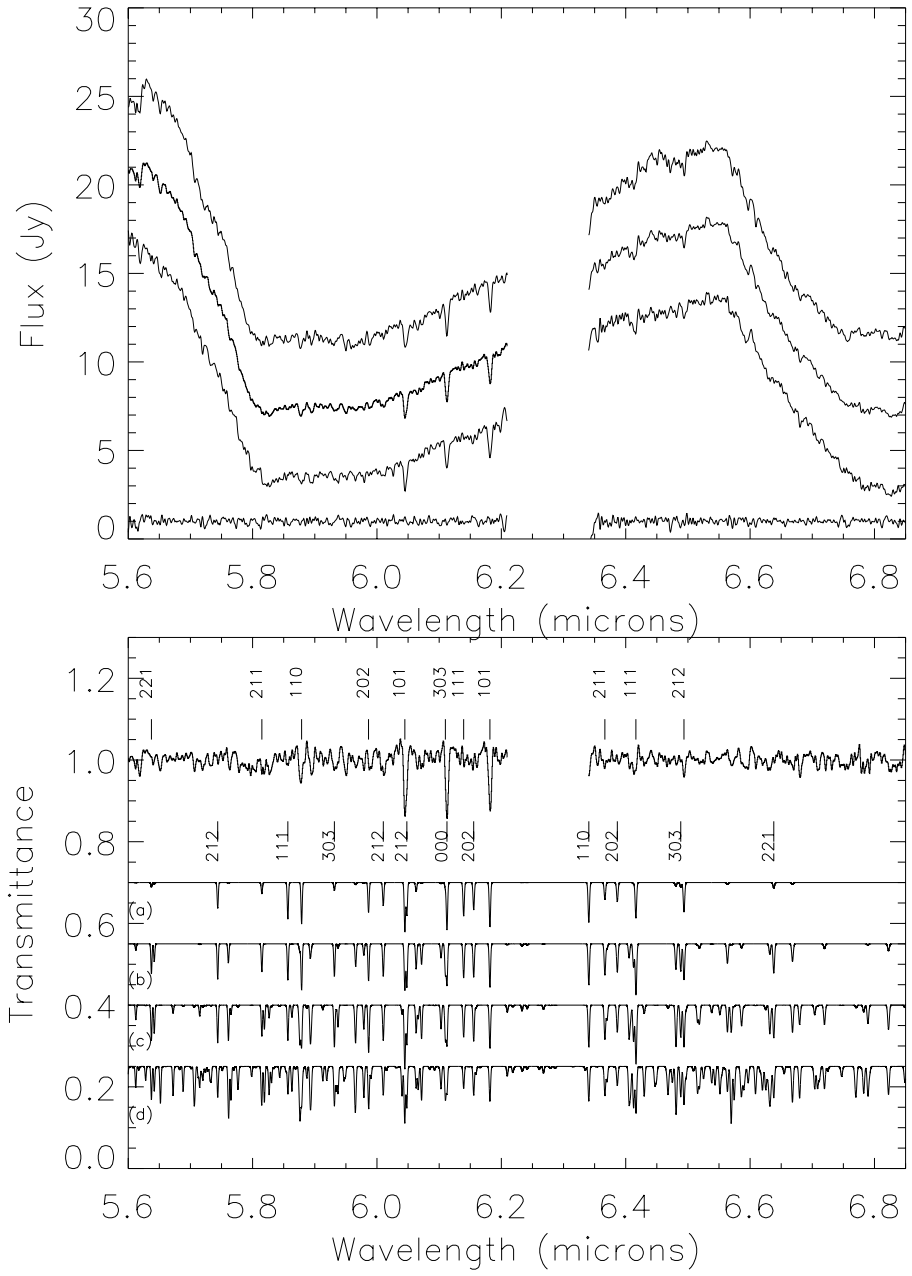

Fig. 9. Upper panel: upward scans, all scans, downward scans and high frequency signal obtained on the difference between upward and downward scans divided by $\sqrt{2}$ to estimate the noise on the spectra. Lower panel: Gas phase H_2O ν_2 band Observed in RAFGL 7009S and model spectra with v= 3 km.s^{-1} and 2×10^{18}cm^{-2} at temperature (a) T=25K (b) T=50K (c) T=100K (d) T=300K. Assignment of the pure rotational levels from which transitions comes from have been made for the strongest bands occurring at T=50K, showing that we mainly deal with a cold component of the gas.

objects. Clearly, CO_2 is much more abundant in the solid than in the gas phase.

3.3. Gas phase H_2O band

As for CO_2, the H_2O ν_2 band is detected in our spectra of RAFGL 7009S, but the rotation-vibration bands seen in absorption span a wider range ($\sim$ 5.5μm to 6.9μm) , compared to carbon dioxide, since the molecule is lighter. Ortho and para H_2O lines are observed, some of which are saturated. We use the same modelling methods as for CO_2. The temperature estimate from individual lines seems rather difficult to obtain. When choosing the strongest lines to make a rotation diagram one is limited by saturation effects and, taking the non-saturated ones, one is limited by the signal-to-noise ratio. Nevertheless, a tentative assignment of the observed lines can give information on the range of temperatures reached by the gas.

In Fig. 9 it can be seen that the strongest observed transitions coincide with low level rotational lines (ground, J=1 or J=2 levels). A comparison of the data and the model spectra allows us to exclude dominant absorption from gas hotter than about 50 K. The spectrum between e.g. 5.65 and 5.75 or 5.9 and 6 μm would present many more lines than observed if the gas were at a higher temperature as clearly evidenced in the results of Helmich et al. (1996). We then propose that most of the water vapor lies at temperatures between 20 and 50K in what we call the cold component. We cannot exclude the possibility of a hot component that could be responsible for a few lines that

seem to be present (with a high J), however these would have a much lower column density. This maximum column density can be estimated because no lines (except the three prominent fundamentals) have a transmittance lower than 0.94. Using a b parameter of 3 km.s^{-1} and temperatures between 300K and 740K for the possible H_2O hot component we derive an upper limit to this component of at least a factor of 3 below the cold one. This will be worse (i.e. it will imply lower column densities) if the hot component has a greater turbulent velocity. However, the signal-to-noise ratio does not allow us to draw firmer conclusions.

3.4. Gas phase CH_4 ν_2/ν_4 dyad

Methane is a molecule pertaining to the T_d point group and is therefore inactive in its rotational ground state mode and thus not observable in the radio range. CH_4 can then only be clearly seen through the rovibrational modes (Boogert et al., 1997) such as the ν_2/ν_4 dyad falling in the 7.7 μm range. One of the surprises of the observations is the ease with which those gas phase lines are detected superimposed on the CH_4 ice feature. We present the CH_4 analysis in Fig. 11, using a slighlty different approach from the one adopted for CO_2 and H_2O. Indeed, we use a real laboratory UV photolysed ice spectrum obtained from a mixture (H_2O,CO,CH_4,NH_3,O_2:15,8,3,2.75,5) to provide the synthetic spectrum (see panel A). The gas phase model spectrum is generated using the extensive list of weighted squared transition moments for the ν_2/ν_4 dyad given in the HITRAN database. We deduce from this data the oscillator strength of each line. The population of the ground state is given in LTE by the formula:

$$N_J = g_N \; g_I \; e^{-\frac{hc\sigma_J}{kT}}/Q_r(T)$$

Where g_N = 5, 3, 2 for symetry A, E and F and Q_r is the rotational partition function given by:

$$Q_r(T) = \Sigma_J \; g_N \; g_I \; e^{-\frac{hc\sigma_J}{kT}}$$

Assuming a doppler parameter and a line profile, as given for H_2O data, a model can be made and compared to observations. The best fit spectrum is obtained with a column density of $1.2^{+0.5}_{-0.3}.10^{17}$cm^{-2} with a temperature of about 50 K and is shown in Fig 11b. The ratio of gas to solid methane is then 0.23, similar to that for H_2O but significantly different from CO_2. Finally, although we choose not to discuss the solid state effects here, we wish to emphasize that, for CH_4, a non polar molecule which is not disturbed by its environment, a quasi-exact match between the laboratory data and the observed feature is obtained, showing that grain size effects or shapes are unimportant for this molecule at this wavelength, thus validating our laboratory simulations. This aspect will be discussed in a forthcoming paper.

4. Discussion

In Table 2 the column densities estimated from the data analysis are summarized. The CO lines clearly show two different temperatures. The ISO-SWS beam does not allow us to separate them spatially. It is likely that the warm gas is associated with the high velocity molecular outflow detected in ^{12}CO $1 \rightarrow 0$ (Shepherd and Churchwell et al., 1996). The presence of this huge amount of hot CO in the line of sight and the fact that we do not clearly see a hot H_2O, CO_2 or CH_4 component might be explained as following: CO is a quite stable molecule and it must be considered as non directly comparable to other species. We hope that the outflow dynamical timescale (1.8×10^4 years) is small enough so that the bulk of the quiescent cocoon surrounding the source has not been chemically perturbed. We trust that we can use our data to obtain some quantitative insight into the role of grains in interstellar chemistry in the dark and cold molecular region surrounding the hot core.

The absorption spectra of all gas phase species imply the existence of a relatively low temperature component ($\sim$50K). Apart from CO, the cold component is the dominant one. This is in contrast with other observations of young embedded stellar objects for which water vapor is observed at about 300 K (van Dishoeck et al. 1996). An important question is to know whether water forms on grains or in the gas. The formation of H_2O molecule in the gas phase involves reactions with activation energies. The high abundance of water ice in dark clouds such as

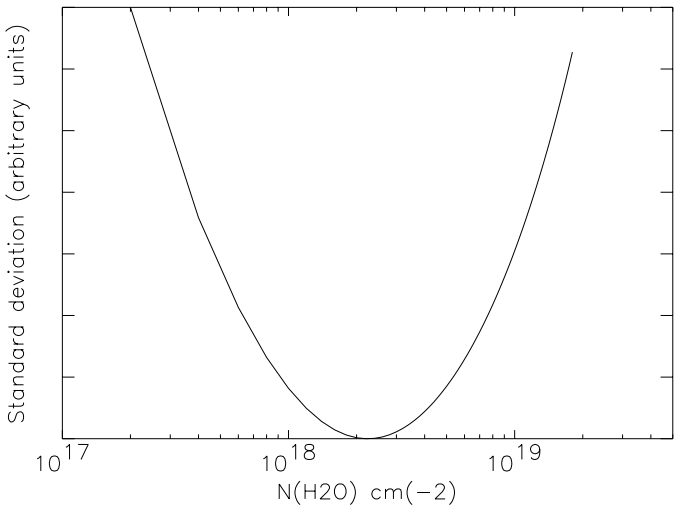

Fig. 10. Correlation diagram made on the result of the division between observations and models spectra for H_2O generated with a b parameter of 3 km.s^{-1}, T=40K and various column densities. The variance reach a minimum for 2×10^{18} molecules cm^{-2} but due to the lowering of sensitivity of this approach at higher column densities due to saturation effects, we choose to put only a lower limit on the column density derived.

Table 2. Gas to solid ratios in RAFGL 7009S (Solid phase values are taken from d'Hendecourt et al. 1996).

	$Gas\ cm^{-2}$	$Solid\ cm^{-2}$	$Gas/Solid$
H_2O	$\geq 2 \times 10^{18}$	1.1×10^{19}	≥ 0.18
CO_2	$1.0^{+1}_{-0.5} \times 10^{17}$	2.5×10^{18}	~ 0.04
CH_4	$1.2^{+0.5}_{-0.3} \times 10^{17}$	4.3×10^{17}	~ 0.28
CO	$6.1^{+1.7}_{-1.7} \times 10^{18}$ $(cold\ component)$	1.8×10^{18}	~ 3.4

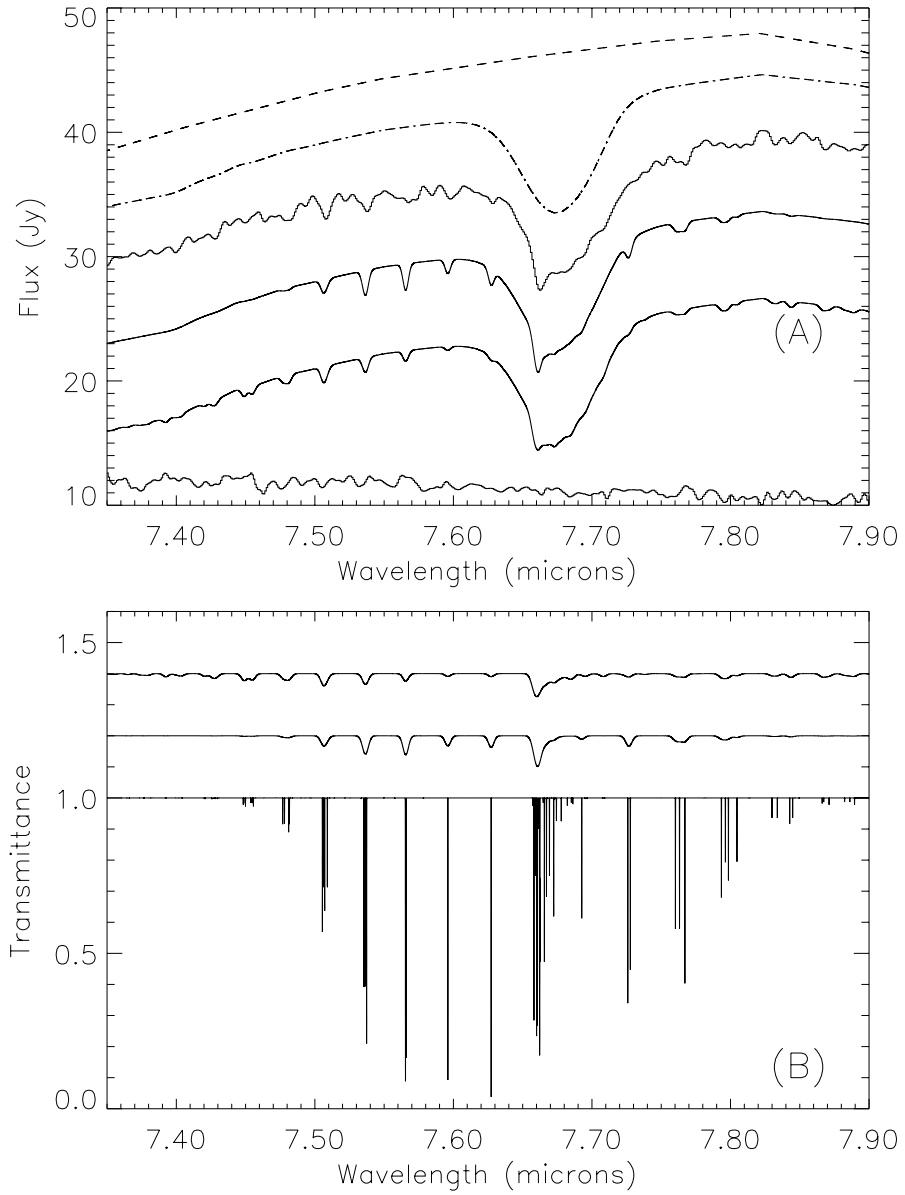

Fig. 11a and b. Gas phase CH_4 for the ν_2/ν_4 dyad. **a** From upper to lower curve, continuum adopted, resultant spectrum with the CH_4 laboratory ice feature, ISO spectrum of RAFGL 7009S, spectra when both gas phase model (respectively 50 and 200K) and laboratory spectrum are taken into account and difference between upward and downward scans divided by $\sqrt{2}$ to estimate the noise level. Even the broad absorption around 7.4 μm seems to be reproduced by laboratory experiment. **b** Model spectrum with T = 200 K, doppler parameter b = 3 km.s^{-1} and a column density of 10^{17}cm^{-2} at R=1800. Model spectrum with T = 50 K, doppler parameter b = 3 km.s^{-1} and a column density of 10^{17}cm^{-2} at R=1800. Full resolution for the second spectrum is shown.

Taurus (10% of the cosmic oxygen abundance in H_2O, Whittet et al. 1988) is not reproduced by chemistry models assuming formation in the gas followed by accretion on dust. Formation on grain surfaces therefore seems required. Most models including water formation on grain surfaces predict H_2O rich mantles (Tielens and Hagen 1982, d'Hendecourt et al. 1985, Hasegawa et al. 1992, Bergin et al. 1995), water being in most cases the dominant solid state species. The main result about water from our observations is that most of the water is in the solid phase. This strongly argues for the formation on dust and we believe that the cold gas phase water is desorbed from grains.

It is generally accepted that gas phase chemical models cannot reproduce the observed amounts of CO_2 on grains. Laboratory experiments (d'Hendecourt et al. 1986) show that CO_2 is efficiently produced by UV photolysis of ices containing CO, H_2O and/or O_2, as well as by cosmic ray irradiation. Surface reactions have also been proposed as an important formation process (Tielens and Hagen, 1982).

The grain/gas abundance ratio is significantly higher for CO_2 (by a factor 4 to 7) than it is for H_2O and CH_4. This result might be taken as evidence that CO_2 is essentially produced on grains and is rapidly destroyed in the gas phase. Indeed CO_2 reacts with H^+,H_2^+ or H_3^+ to form HCO^+ or HCO_2^+ ions. High abundances of these ions in some sources may be a direct evidence for the release of grain species into the gas phase as noted by Breukers (1991) and Breukers et al. (1992).

If the observed molecules are efficiently formed on grains, the grain/gas abundance ratio provides information on the desorption mechanism. The gas to solid ratio is comparable for methane and water given that these molecules have different condensation temperatures. This ratio will depend on specific destruction routes once the molecules are released in the gas.

This may be further investigated with models using gas and grain chemistry together.

The methane desorption can help to feed the backend of the ladder for the formation of more complex hydrocarbons detected at radio wavelength in the gas phase as was pointed out in the model of Brown and Charnley (1991). Such models will help to constrain desorption mechanisms. Cosmic ray induced desorption (Léger et al, 1985) together with chemical explosions (d'Hendecourt et al., 1982) are plausible and need also to be investigated by further laboratory work.

5. Conclusion

We have presented ISO-SWS results on a protostellar source in which the solid phase abundance is dominating the spectra. Superimposed on the solid state features, gas phase molecules were observed allowing the estimate of gas to solid ratios. Except for CO, they are all in favour of the solid phase and CO_2 is particularly deficient in the gas. Furthermore, the quite low temperatures derived for the gas are not in aggreement with the massive formation of H_2O in the gas as activation barriers are involved in the process. However, if the molecules are effectively formed on grains, desorption mechanism must be an out-of-equilibrium process.

Acknowledgements. We wish to thank Dominique Bocklée-Morvan and Guillaume Pineau des Forêts for fruitful discussions. We are grateful to the referee Dr Xander Tielens for greatly improving the manuscript.

References

Bergin E. A., Langer W. D., Goldsmith P. F., 1995, A&A 441, 222.
Boogert A. C. A., Schutte W. A., Helmich F. P., Tielens A. G. G. M., Wooden D. H., 1997, A&A 317, 929.
Breukers R. J. L. H., thesis, University of Leiden, 1991.
Breukers R. J. L. H., d'Hendecourt L. B., Greenberg J. M., in Chemistry and Spectroscopy of Interstellar Molecules, PACIFICHEM international symposium, Edited by Diethard K. Bohme, Eric Herbst, Norio Kaifu, Shuji Saito, University of Tokyo press.
Brown P. D. and Charnley S. B., 1991, MNRAS 249, 69.
Van Dishoeck E. F. and Helmich F. P. 1996, A&A 315, L177.
Van Dishoeck E. F., Helmich F. P., de Graauw Th., Black J.H. et al., 1996, A&A 315, L349.
Geballe T. R.,Baas F., Greenberg J. M., Schutte W., 1985, A&A 146, L6.
Gerakines P. A., Schutte W. A., Greenberg J. M., van Dishoeck E. F., 1995, A&A 296, 810.
De Graauw T., Haser L. N., Beintema D. A., Roelfsema P. R., Van Agthoven H. et al., 1996, A&A 315, L49.
Hasegawa T. I., Herbst E., Leukng C. M. , 1992, ApJS 82, 167.
Helmich F. P., Van Dishoeck E. F., Black J. H. et al., 1996, A&A 315, L173.
d'Hendecourt L. B., Allamandola L. J., Baas F., Greenberg J. M., 1982, A&A 109, L12.
d'Hendecourt L. B., Allamandola L. J., Greenberg J. M., 1985, A&A 152, 130.
d'Hendecourt L. B., Allamandola L. J., Grim R. J. A., Greenberg J. M., 1986 A&A 158, 119.
d'Hendecourt L. B. and Jourdain de Muizon M., 1989, A&A 223, L5.
d'Hendecourt L., Jourdain de Muizon M., Dartois E., Breitfellner M. et al., 1996, A&A 315, L365.
Kessler M.F., Steinz J.A., Anderegg M.E. et al., 1996, A&A 315, 27.
Léger A., Jura M., Omont A., 1985, A&A 144, 147.
McCutcheon W.H., Dewdney P.E., Purton C.R., Sato T., 1991, AJ 101, 1435.
McCutcheon W.H., Sato T., Purton C.R., Matthews H.E., Dewdney P.E., 1995, AJ 110, 1762.
Minh Y. C., Irvine W. M., Ziurys L. M., 1988,ApJ 334, 175.
Mitchell G.F., Maillard J.-P., Allen M., Beer R., Belcourt K., 1990, ApJ 363, 554.
Reichle H.G., Young C., 1972, Canadian Journal of Physics 50, 2662.
Rothman L. S., Gamache R. R., Tipping R. H. et al., 1996, J. Quant. Spectrosc. Radiat. Transfer 48, 469.
Shepherd D. S. and Churchwell E., 1996, AJ 457, 267.
Tielens A. G. G. M. and Hagen W., 1982, A&A 114, 245.
Whittet D. C. B., Bode M. F., Longmore A. J., Admason A. J. et al., 1988, MNRAS 233, 321.

This article was processed by the author using Springer-Verlag LaTeX A&A style file *L-AA* version 3.